

Rotational spectroscopy of interstellar PAHs

Yacine Ali-Haïmoud*

Institute for Advanced Study, Einstein Drive, Princeton, New Jersey 08540

7 June 2018

ABSTRACT

Polycyclic aromatic hydrocarbons (PAHs) are believed to be ubiquitous in the interstellar medium. Yet, to date no specific PAH molecule has been identified. In this paper, a new observational avenue is suggested to detect individual PAHs, using their rotational line emission at radio frequencies. Previous PAH searches based on rotational spectroscopy have only targeted the bowl-shaped corannulene molecule, with the underlying assumption that other polar PAHs are triaxial and have a complex and diluted spectrum unusable for identification purposes. In this paper the rotational spectrum of quasi-symmetric PAHs is computed analytically. It is shown that the asymmetry of planar, nitrogen-substituted symmetric PAHs is small enough that their rotational spectrum, when observed with a resolution of about a MHz, has the appearance of a “comb” of evenly spaced stacks of lines. The simple pattern of these “comb” spectra allows for the use of matched-filtering techniques, which can result in a significantly enhanced signal-to-noise ratio. Detection forecasts are discussed for regions harbouring “anomalous microwave emission”, believed to originate from the collective PAH rotational emission. A systematic search for PAH lines in various environments is advocated. If detected, PAH “combs” would allow to the conclusive and unambiguous identification of specific, free-floating interstellar PAHs.

Key words: ISM: dust

1 INTRODUCTION

Polycyclic aromatic hydrocarbons (PAHs) are believed to be ubiquitous in the interstellar medium (ISM). They are estimated to contain several percent of the total interstellar carbon, which translates to a typical abundance of a few times 10^{-7} PAH per hydrogen atom for a characteristic number of 50 carbon atoms per molecule, making PAHs, as a family, one of the most abundant molecular species in the ISM. They play important roles in the physics and chemistry of the ISM, influencing, and sometimes controlling, the ionisation balance and the photoelectric heating (for a recent review, see Tielens 2008; see also Draine 2011). The presence of these large carbonaceous compounds in the ISM is strongly hinted at, if not required, by various otherwise “unidentified” or “anomalous” emission and absorption features throughout the electromagnetic spectrum. First and foremost, there is now general agreement for attributing the infrared emission features at 3–19 μm to PAH vibrational transitions following transient heating to high temperatures by ambient ultraviolet (UV) photons (Puget & Leger 1989; Allamandola et al. 1989), even though this

is still the subject of occasional heated debates (Kwok & Zhang 2011; Li & Draine 2012; Kwok & Zhang 2013). Second, electronic transitions of ionised PAHs could be at the origin of the diffuse interstellar bands (DIBs) in the visible (Leger & D’Hendecourt 1985; Crawford et al. 1985; van der Zwet & Allamandola 1985), though the case is not fully settled (Tielens 2008). The “extended red emission” could be the counterpart of the DIBs in emission, and PAHs have also been suggested as its carriers (Witt et al. 2006). Third, the best candidate for the cm-wavelength “anomalous” dust-correlated emission is rotational emission from very small spinning dust grains (Draine & Lazarian 1998a,b), at the very least for the lack of better candidates (with the exception of magnetic dipole radiation suggested by Draine & Lazarian (1999), though a recent re-investigation of the problem by Draine & Hensley (2013) suggests typical radiation frequencies higher than the observed anomalous emission), and also because observations seem to fit well theoretical models, see for example Scaife (2013) and references therein. These various aspects make a strong case for the PAH hypothesis, further reinforced by their expected stability under the harsh interstellar UV radiation if they contain ~ 20 carbon atoms or more (Leger & D’Hendecourt 1985). And yet, specific PAHs have eluded detection thus far, which

* E-mail: yacine@ias.edu

is one of the main arguments of the PAH-hypothesis opponents (Kwok & Zhang 2011, 2013). It is indeed difficult to extract information about individual carriers from the infrared emission features, which are mostly due to nearest-neighbour vibrations, and there is currently little data at the far-infrared frequencies, which correspond to the bending modes of the skeleton and could trace specific molecules (Tielens 2008; Zhang et al. 2010).

Rotational spectroscopy is routinely used to identify molecules in space, and it is natural to ask whether this technique can be used for PAHs. Suggestions to do so can be found in a few places in the literature (Hudgins et al. 2005; Tielens 2008; Hammonds et al. 2011), but so far the only PAH that has been searched for using its rotational emission is the polar, bowl-shaped corannulene molecule $C_{20}H_{10}$. Its rotational constants were measured by Lovas et al. (2005), whose results were used by Thaddeus (2006) and Pilleri et al. (2009) to set an upper bound to the fraction of interstellar carbon locked in corannulene of $\sim 10^{-5}$ and $\sim 2 \times 10^{-6}$, respectively, which are much smaller values than the estimated $\sim 10\%$ fraction of carbon locked in PAHs. These results only apply to specific lines of sight, however, and to a very specific PAH which may simply not be efficiently formed in the ISM or may be too small to be stable under the harsh UV background. A search for rotational transitions of other PAHs has never been carried out, however, due to the following *a priori* difficulties. Firstly, the number of possible configurations with a few tens of carbon atoms is a priori gigantic (Salama et al. 1996), and it could very well be that no specific species is abundant enough that it could ever be detected, with any method (this could explain the very low upper bounds on the abundance of corannulene). That being said, the more compact, “pericondensed” configurations are more stable than the more linear, “cata-condensed” forms (Ricca et al. 2012), and it is conceivable that only a limited number of stable species dominate the PAH population (“grandPAHs”, in the words of A. Tielens). In fact, comparison of theoretical infrared spectra with observations do suggest that interstellar PAHs are rather compact and symmetric (Bauschlicher et al. 2009). Moreover, the presence of a limited number of features, both in the mid-IR spectrum and in the DIBs, suggests that their population is, indeed (provided they are the carriers of these features), dominated by a relatively small number of definite species (Salama et al. 1996; Boersma et al. 2010; Ricca et al. 2012), though this statement has never been made fully quantitative. Secondly, ideal PAHs are not necessarily polar, especially the highly symmetric ones that are the most likely to be overabundant. If this is the case they cannot radiate through rotational transitions. Interstellar PAHs are however likely to have some form of impurity (dehydrogenation, super-hydrogenation, substitution...) that would endow them with a permanent dipole moment. Finally, the PAHs that are polar are in general triaxial molecules (except for very special cases like that of corannulene), either because of their intrinsic geometry, or because of the very impurities that make them polar and break their symmetry even if they are initially perfectly symmetric. The power radiated by large triaxial molecules is in general diluted between a very large number of weak lines, which may disappear in the grass and be of little use for identification purposes (Tie-

lens 2008). This last point, however, has never been made quantitative, which is one of the goals of the present work.

In this paper, we first compute the emission spectrum of *quasi-symmetric* rotors using quantum mechanical perturbation theory (Section 2). We show that for a small enough degree of asymmetry, the rotational spectrum of a planar PAH, observed with a few MHz resolution, has the appearance of a “comb” with evenly spaced “teeth”, each one of which being really a stack of a large number of transitions that fall at nearly identical frequencies. We then quantify the level of asymmetry of realistic PAHs with various imperfections in Section 3. We show in particular that nitrogen-substituted PAHs (PANHs), which are strongly polar and are believed to be a significant fraction of the interstellar PAH population (Hudgins et al. 2005), do remain symmetric enough to have a “comb” spectrum. They therefore make a promising target for PAH rotational spectroscopy. The very distinctive pattern of such “comb” spectra allows for the use of matched-filtering techniques to blindly search for specific PAHs with unknown size, as we describe in Section 4. Such techniques could allow for the statistical detection of combs, even if none of the lines are strong enough to be detected on their own. We make rough detection forecasts in Section 5, based on the observed amplitude of the “anomalous microwave emission” (AME), assuming it is the broadband and collective rotational emission from PAHs. Our estimates indicate that the detection of individual PAHs with current radio telescopes may be challenging but remains possible provided the fraction of PAHs in a particular species is large enough (typically of order a percent, but possibly less). We advocate for a systematic search of PAH rotational lines in large bandwidth, few MHz resolution radio spectra of regions with known anomalous microwave emission, as well as in regions with known or potential large PAH abundances. Protoplanetary or planetary nebulae also make interesting targets, and the detection of individual PAHs in these regions would shed light on the route to large organic molecules and constrain chemical models (Kwok 2004). Detection of PAH rotational lines would be a smoking-gun confirmation of their existence as free-floating molecules in the interstellar medium, and would allow to finally identify individual species, a nagging missing piece to the otherwise very appealing PAH hypothesis.

2 ROTATIONAL LINE EMISSION FROM QUASI-SYMMETRIC PLANAR PAHS

2.1 Motivations

An ideal planar rigid symmetric top emits a series of evenly spaced rotational lines, with a line spacing $\Delta\nu_{\text{line}} = \hbar/(2\pi I_3)$, where I_3 is the largest moment of inertia, which is precisely twice as large as the other two equal moments of inertia. Each line is in fact a “stack” from $\sim J_0$ different transitions with equal frequencies, where J_0 is the characteristic total angular momentum quantum number. We show approximate values of $\Delta\nu_{\text{line}}$ for selected symmetric PAHs in Table 1. Note that this table is neither exhaustive nor very accurate and only serves the purpose of illustration.

On the other hand, and as we shall illustrate below, a large triaxial molecule has a complex rotational spectrum,

with no closed-form expression, for which the line spacing is uneven and, more importantly, for which different transitions do not in general fall at the same frequency. The power is therefore diluted over a large number of lines with respect to the symmetric case and decreased by a factor of order $J_0 \sim 100$ for the smallest grains, this number increasing with grain size. This decreased power per line (the lines actually blur into a quasi-continuum for large molecules), and the additional complication in the computation of the exact spectrum, concur in making the search for specific molecules much more difficult if they are triaxial than if they are symmetric. We must therefore focus our attention on symmetric PAHs if we hope to achieve any detection through rotational spectroscopy.

But how symmetric can real *radiating* PAHs be? In order to radiate, a rotating grain must have a permanent dipole moment. A few PAHs like corannulene ($C_{20}H_{10}$) do possess such a permanent dipole moment because of their non-planarity. Symmetric non-planar PAHs nevertheless probably constitute an even smaller fraction of the PAH family. For planar PAHs, on the other hand, a permanent dipole moment must come from some imperfection in the grain. Besides the restricted case where the dipole moment arises from an association with a metal complex outside of the plane and aligned with the grain's axis of symmetry, most imperfections leading to a dipole moment (superhydrogenation, de-hydrogenation, substitution of a carbon atom by a nitrogen atom, etc...) will invariably break the symmetry of the inertia tensor at some level. How exactly this affects the rotational spectrum is a quantitative question, which we address in this section.

Before moving on to the computation, we point out that we shall assume PAHs to be *rigid* rotors. Laboratory studies of corannulene indeed show no significant centrifugal distortion to its rotational spectrum (Lovas et al. 2005; Pilleri et al. 2009). Since small PAHs spend a very large fraction of their time in their vibrational ground state, we shall moreover assume that they are described by a single set of rotational constants.

2.2 Perturbed quantum-mechanical rigid symmetric top

Computing the transition frequencies and line intensities of a triaxial quantum-mechanical rotor does not present any major conceptual difficulty, see for example van Winter (1954). However, there are no closed form solutions to this problem. In order to understand the effect of a small degree of triaxiality analytically, we treat the problem perturbatively, assuming a small departure from a rigid symmetric-top rotor. This allows us to write down closed-form expressions for the rotational transitions.

We consider a rigid triaxial rotor with principal moments of inertia I_i and angular momentum operators along the principal axes L_i . Its rotational hamiltonian is

$$H = \sum_i \frac{L_i^2}{2I_i} \equiv \frac{2\pi}{h} \sum_i A_i L_i^2 \quad (1)$$

where $\hbar = h/(2\pi)$, h being the Planck constant, and the A_i are the rotational constants, which have the dimension of a frequency:

$$A_i \equiv \frac{h}{8\pi^2 I_i}. \quad (2)$$

Here we shall assume for definiteness $I_1 \leq I_2 < I_3$, i.e. $A_1 \geq A_2 > A_3$. A nearly symmetric oblate top has $A_1 \approx A_2$. Defining

$$\bar{A}_{12} \equiv \frac{A_1 + A_2}{2}, \quad (3)$$

we rewrite the Hamiltonian in the form

$$\begin{aligned} \frac{\hbar}{2\pi} H &= A_3 L_3^2 + \bar{A}_{12} (L_1^2 + L_2^2) + \frac{A_1 - A_2}{2} (L_1^2 - L_2^2) \\ &= \bar{A}_{12} L^2 - (\bar{A}_{12} - A_3) L_3^2 + \frac{A_1 - A_2}{2} (L_1^2 - L_2^2), \end{aligned} \quad (4)$$

where $L^2 \equiv \sum_i L_i^2$. We recognise this expression as the sum $H = H^0 + V$ of the hamiltonian H^0 of a symmetric rotor with rotational constants $A'_1 = A'_2 = \bar{A}_{12}$ and $A'_3 = A_3$, and a perturbation V such that

$$\frac{\hbar}{2\pi} V \equiv \frac{A_1 - A_2}{2} (L_1^2 - L_2^2) \equiv \epsilon (\bar{A}_{12} - A_3) (L_1^2 - L_2^2), \quad (5)$$

where we have defined our perturbation parameter as in Townes & Schawlow (1975):

$$\epsilon \equiv \frac{A_1 - A_2}{A_1 + A_2 - 2A_3}. \quad (6)$$

The eigenfunctions of the unperturbed hamiltonian H^0 are the wavefunctions $|JKM\rangle$, with total angular momentum $L^2 = \hbar^2 J(J+1)$, angular momentum along the e_3 axis $L_3 = \hbar K$ and angular momentum along some fixed direction in space $L_z = \hbar M$, where J, K, M are integers and $-J \leq K, M \leq J$. The corresponding unperturbed eigenvalues are

$$E_{JK}^0 = h [\bar{A}_{12} J(J+1) - (\bar{A}_{12} - A_3) K^2]. \quad (7)$$

The perturbation hamiltonian can be rewritten in terms of the operators $L_{\pm} \equiv L_1 \mp iL_2$ as follows:

$$\frac{\hbar}{2\pi} V = \frac{\epsilon}{2} (\bar{A}_{12} - A_3) (L_+^2 + L_-^2). \quad (8)$$

The operators L_{\pm} are the raising and lowering operators for the projection of the angular momentum along e_3 (van Winter 1954; Edmonds 1960):

$$L_{\pm} |JKM\rangle = \hbar [J(J+1) - K(K \pm 1)]^{1/2} |J(K \pm 1)M\rangle. \quad (9)$$

The only non-vanishing matrix elements of the perturbation are therefore

$$\begin{aligned} \langle J(K \pm 2)M | V | JK M \rangle &= h \frac{\epsilon}{2} (\bar{A}_{12} - A_3) \\ &\times [J(J+1) - K(K \pm 1)]^{1/2} [J(J+1) - (K \pm 1)(K \pm 2)]^{1/2}. \end{aligned} \quad (10)$$

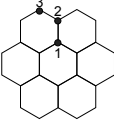
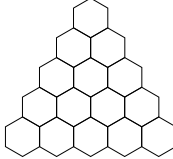
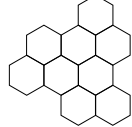
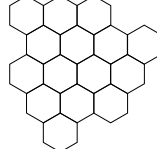
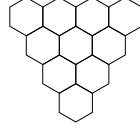
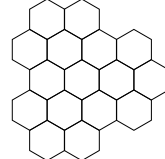
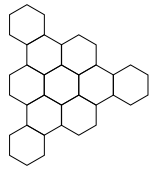
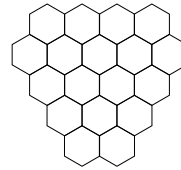
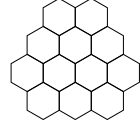
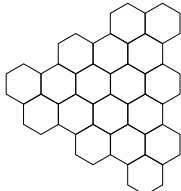
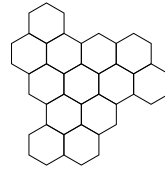
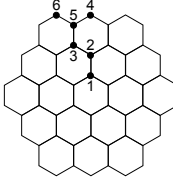
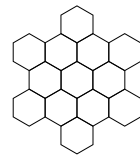
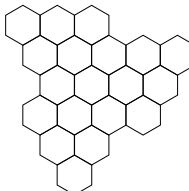
For a given J and M , the states $\pm K$ (with $K \neq 0$) are degenerate for the unperturbed hamiltonian, and the second-order corrections to the energy levels, δE , are given by solving the secular equation (Landau & Lifshitz 1965):

$$\det \left[V_{K_1, K_2} + \sum_{K' \neq \pm K} \frac{V_{K_1, K'} V_{K', K_2}}{E_{JK}^0 - E_{JK'}^0} - \delta E \delta_{K_1, K_2} \right] = 0, \quad (11)$$

where $K_1, K_2 = \pm K$, $V_{K, K'} \equiv \langle JK M | V | JK' M \rangle$ and the above equation is to be understood as a 2 by 2 determinant in the subspace spanned by $|JKM\rangle$ and $|J(-K)M\rangle$.

Let us first consider the subspace spanned by $K = \pm 1$.

Table 1. Approximate line spacing $\Delta\nu_{\text{line}} = 2A_3$ for a few symmetric PAHs. They were computed assuming a perfectly hexagonal carbon skeleton with a C-C bond length of 1.4 Å and a C-H bond length of 1.1 Å for the peripheral hydrogen atoms (not shown). Numbers on coronene and circumcoronene label the non-equivalent sites for single substitution of a carbon atom by a nitrogen atom.

Structure	Formula	Line spacing (MHz)	Structure	Formula	Line spacing (MHz)
	C ₂₄ H ₁₂ (coronene)	340		C ₄₆ H ₁₈	83.0
	C ₃₁ H ₁₅	192		C ₄₆ H ₁₈	89.0
	C ₃₃ H ₁₅	164		C ₄₈ H ₁₈	83.1
	C ₃₆ H ₁₈	128		C ₅₂ H ₁₈	70.7
	C ₃₇ H ₁₅	142		C ₅₅ H ₂₁	59.3
	C ₄₂ H ₁₈	101		C ₅₄ H ₁₈ (circumcoronene)	67.6
	C ₄₂ H ₁₈	108		C ₅₇ H ₂₁	54.8

Since the matrix element $V_{1,-1}$ is non zero, the energy shift is of first order in the perturbation parameter. The proper eigenfunctions are

$$|J1_{\pm}\rangle \equiv \frac{1}{\sqrt{2}} (|J(+1)M\rangle \pm |J(-1)M\rangle), \quad (12)$$

which have perturbed energies given by, to lowest order,

$$\delta E_{J,1_{\pm}} = \pm h \frac{\epsilon}{2} (\bar{A}_{12} - A_3) J(J+1). \quad (13)$$

We now consider the subspace spanned by $K = \pm 2$. Here the matrix element $V_{-2,+2}$ does vanish so the perturbation is of second order. Again, one can show that the eigenfunctions of the perturbed hamiltonian are

$$|J2_{\pm}\rangle \equiv \frac{1}{\sqrt{2}} (|J(+2)M\rangle \pm |J(-2)M\rangle), \quad (14)$$

with perturbed energies such that

$$\frac{\delta E_{J,2+}}{h(\bar{A}_{12} - A_3)} = -\frac{\epsilon^2}{8} \left[\frac{5}{6} J^2 (J+1)^2 + J(J+1) - 12 \right], \quad (15)$$

$$\frac{\delta E_{J,2-}}{h(\bar{A}_{12} - A_3)} = \frac{\epsilon^2}{8} \left[\frac{1}{6} J^2 (J+1)^2 - 3J(J+1) + 12 \right]. \quad (16)$$

Finally, for $|K| \neq 1, 2$, the eigenfunctions $|JKM\rangle$ constitute an appropriate basis for perturbation theory (i.e. the exact eigenfunctions are only perturbatively different from them), and the energy shifts are of second order in ϵ and given by

$$\frac{\delta E_{JK}}{h(\bar{A}_{12} - A_3)} = -\frac{\epsilon^2}{8} \left[\frac{J^2 (J+1)^2}{K^2 - 1} + 2J(J+1) - 3K^2 \right]. \quad (17)$$

This formula is also valid for $K = 0$. Splitting of the $\pm K$ degenerate eigenstates only enters through higher-order corrections for $|K| \neq 1, 2$. We have checked that our expressions (13), (15) (16) and (17) coincide with exact expressions for the energy levels of an asymmetric top computed for low J -values, when Taylor-expanded in the asymmetry parameter. Such expressions can be found in Chapter 4 of Townes & Schawlow (1975), for example.

For large J , and $K \sim J$ this expression is of order $\delta E_{JK} \sim \epsilon^2 E_{JK}^0$, as one would expect. For $1 \ll |K| \ll J$, using $A_1 \approx A_2 \approx 2A_3$ for a planar grain, we have, to lowest order,

$$\frac{\delta E_{JK}}{E_{JK}^0} \approx -\frac{\epsilon^2}{16} \frac{J^2}{K^2}. \quad (18)$$

This means that perturbation theory is valid only as long as $K \gg (\epsilon/4)J$. In practice, we will consider typically $\epsilon \sim 10^{-3} - 10^{-2}$ and $J \sim 10^2 - 10^3$ so the perturbation theory results might only break down for the smallest few values of K and quickly becomes very accurate as $|K|$ increases.

2.3 Application to a planar grain

We now specialise to a *planar* grain. For a classical rigid planar object with normal along e_3 , the moments of inertia are related by $I_3 = I_1 + I_2$. However, this relation is not exact for a quantum-mechanical object due to zero-point fluctuations and vibration-rotation interactions (i.e. not perfect rigidity). We denote by δ the dimensionless inertial defect quantifying the departure from this relation:

$$\delta \equiv \frac{I_3 - I_1 - I_2}{I_3}. \quad (19)$$

This quantity can have either sign and is small, $|\delta| \ll 1$.

With this definition and that of ϵ , (Eq. 6), we may rewrite A_1 and A_2 , to second order in ϵ and first order in δ , in terms of A_3 :

$$A_1 \approx \left[2 + \epsilon + \frac{1}{2}\epsilon^2 \right] \frac{A_3}{1 - \delta}, \quad (20)$$

$$A_2 \approx \left[2 - \epsilon + \frac{1}{2}\epsilon^2 \right] \frac{A_3}{1 - \delta} \quad (21)$$

We then re-express the unperturbed energy in the following form, to lowest order in ϵ and δ :

$$\frac{E_{JK}^0}{hA_3} = 2J(J+1) - K^2 + \left(\frac{\epsilon^2}{2} + 2\delta \right) (J(J+1) - K^2). \quad (22)$$

This allows us to rewrite the final energy values as follows, to lowest order in ϵ , and for $|K| \neq 1, 2$:

$$\begin{aligned} \frac{E_{JK}}{hA_3} &= 2J(J+1) - K^2 + 2\delta (J(J+1) - K^2) \\ &- \frac{\epsilon^2}{8} \left(\frac{J^2 (J+1)^2}{K^2 - 1} - 2J(J+1) + K^2 \right). \end{aligned} \quad (23)$$

We have checked that this expression agrees very well with numerical computations for slightly asymmetric tops using the online tool PGOPHER¹ with $J \leq 10$.

2.4 Emission spectrum

Since our expressions are most inaccurate for low values of $|K|$ we shall in what follows only consider transitions involving $|K| \geq 3$, and disregard other transitions. Only a small fraction of the radiated energy is emitted in transitions involving $|K| \leq 2$ for large J , and they therefore only contribute a few weak lines that do not affect observations. This also allows us to easily compute transition rates, since the eigenvalues for $|K| > 2$ are the usual $|JKM\rangle$ with small perturbations.

For the unperturbed symmetric-top, there are four allowed transitions from any given state (J, K) , radiating a power P in the limit² $J, |K| \gg 1$ given by:

$$(J, K) \rightarrow (J-1, K), \quad P = \frac{2\mu_{\text{op}}^2}{3c^3} (2\pi\nu)^4 \left(1 - \frac{K^2}{J^2} \right), \quad (24)$$

$$(J, |K|) \rightarrow (J, |K|+1), \quad P = \frac{\mu_{\text{ip}}^2}{3c^3} (2\pi\nu)^4 \left(1 - \frac{K^2}{J^2} \right), \quad (25)$$

$$(J, K) \rightarrow (J-1, K \pm 1), \quad P = \frac{\mu_{\text{ip}}^2}{6c^3} (2\pi\nu)^4 \left(1 \mp \frac{K}{J} \right)^2, \quad (26)$$

where ν is the frequency of the transition, μ_{op} is the out-of-plane component of the permanent dipole moment (along e_3) and μ_{ip} is its in-plane component.

We will focus our attention on planar substituted PAHs, for which the dipole moment is purely in-plane ($\mu_{\text{op}} = 0$) and the first transition above is not allowed (but there is of course no additional difficulty in considering general orientations of the dipole moment). Also, the $\Delta J = 0$ transition radiates 174 times less power than the $\Delta J = -1, \Delta K = \pm 1$ transition if K is evenly distributed in $[-J, J]$ (Ali-Haïmoud

¹ <http://pgopher.chm.bris.ac.uk/index.html>

² for exact expressions, see for example Ali-Haïmoud (2011)

2011), and radiates no power at all for grains rotating primarily about their axis of greatest inertia. So we only need to focus on the third transition above, Eq. (26). Finally, the perturbed energy levels only depend on the absolute value of K , and the transition $J, K \rightarrow J-1, K+1$ and $J, K \rightarrow J-1, -K-1$ have the same frequency and rate. We therefore only need to account for the $\Delta J = -1, \Delta K = -1$ transitions, provided we double the power given in Eq. (26).

2.5 Impact of defects on the spectrum

A small asymmetry will have two effects. First, it perturbs the eigenfunctions to first order in ϵ . This leads to changes to the rates of the allowed transitions at order ϵ , and to additional transitions with rates proportional to ϵ^2 . These changes are essentially unobservable. The second and most important effect is the change to the transition frequencies. The $\Delta J = -1, \Delta K = -1$ transitions have the following frequencies, to lowest order in ϵ and δ :

$$\begin{aligned} \nu_{J,K} &\equiv \frac{E_{J,K} - E_{J-1,K-1}}{h} = A_3(4J - 2K + 1) \\ &+ A_3 \frac{\epsilon^2}{4} \left(2J - K + \frac{J^3}{K^3} (J - 2K) \right) + 4A_3\delta(J - K), \end{aligned} \quad (27)$$

where we have Taylor-expanded the perturbation parts in $J, |K| \gg 1$, i.e. we are neglecting corrections of order $\epsilon^2 A_3, \delta A_3$ to the transition frequency (typically, if $A_3 \sim 100$ MHz and $\delta \sim \epsilon^2 \lesssim 10^{-4}$, these corrections are of order 0.01 MHz, much smaller than the turbulent velocity broadening). Note that for our numerical computations we use the exact expressions for the energies and transition frequencies.

Let us consider the family of transitions with $K = 2J - J_0$ for $\frac{1}{3}J_0 \leq J \leq J_0$. Their frequencies are

$$\begin{aligned} \nu_{J_0}(J) &\equiv \nu_{J,2J-J_0} = A_3(2J_0 + 1) \\ &+ A_3 \frac{\epsilon^2}{4} (J_0 - J)^3 \frac{3J - J_0}{(2J - J_0)^3} + 4A_3\delta(J_0 - J) \end{aligned} \quad (28)$$

Note that this expression is not valid near $J = J_0/2$ i.e. $K = 0$, since we have derived in it the limit $|K| \gg 1$.

From this expression we can draw several consequences:

(i) In the absence of asymmetry and inertial defect, the above transitions all fall at the same frequency, and appear as a single strong line, which is really a “stack”. These stacks of lines are themselves evenly spaced; their transition energies are a constant times half an integer: $\nu_{J_0} \equiv A_3(2J_0 + 1)$. The rotational spectrum appears as a “comb” with constant spacing $\Delta\nu_{\text{line}} = 2A_3$.

(ii) The effect of the asymmetry alone is to “unfold” each stack of lines into two branches that accumulate near the central frequency $\nu_{J_0, J_0} = \nu_{J_0}$, as the correction term vanishes for $J = J_0 = K$ and $J = J_0/3 = -K$, see top panels of Fig. 1. The two branches correspond to $0 < K \leq J$ (positive frequency offset) and $-J \leq K < 0$ (negative frequency offset). The characteristic spread of the lines, obtained for example by considering the range $-J/2 \leq K \leq J/2$ (corresponding to $\frac{2}{3}J_0 \leq J \leq \frac{2}{3}J_0$) is

$$\Delta\nu \approx \frac{4}{5}\epsilon^2\nu_{J_0}. \quad (29)$$

Therefore the bulk of the lines remain within the same resolution bin of width $\Delta\nu_{\text{res}}$ and the observed aspect of the

spectrum is roughly unchanged from the case $\epsilon = 0$ as long as

$$\epsilon \lesssim \sqrt{\frac{\Delta\nu_{\text{res}}}{\nu}} \approx 10^{-2} \sqrt{\frac{\Delta\nu_{\text{res}}}{3 \text{ MHz}} \frac{30 \text{ GHz}}{\nu}}, \quad (30)$$

For larger asymmetries, the “comb” appearance is preserved but the contrast of the lines decreases with increasing ϵ . For asymmetries greater than

$$\epsilon_{\text{crit}} \approx \sqrt{\frac{\Delta\nu_{\text{line}}}{\nu}} \approx 0.06 \sqrt{\frac{\Delta\nu_{\text{line}}}{100 \text{ MHz}} \frac{30 \text{ GHz}}{\nu}}, \quad (31)$$

each stack of lines is spread over an interval as large as the characteristic line spacing; the spectrum becomes a noisy quasi-continuum essentially unusable for identification purposes. These statements are illustrated in Figs. 1 and 2.

(iii) The effect of the inertial defect alone is to spread the lines of each stack between ν_{J_0} and $\nu_{J_0}(1 + \frac{4}{3}\delta)$ (see Fig. 1). Whereas a small asymmetry could still shift part of the lines very far from their initial frequency (in the limit $|K| \ll J$), an inertial defect spreads the lines over a finite interval of order $\Delta\nu/\nu \approx \delta$. As long as

$$\delta \lesssim \frac{\Delta\nu_{\text{res}}}{\nu} \approx 10^{-4} \frac{\Delta\nu_{\text{res}}}{3 \text{ MHz}} \frac{30 \text{ GHz}}{\nu}, \quad (32)$$

each stack of lines remains clustered within the same resolution element and the observed spectrum is nearly identical to that of a perfectly planar grain. For larger values the spectrum gets spread over a few resolution bins, but still conserves a periodic structure. Only when δ becomes comparable to the critical value

$$\delta_{\text{crit}} \approx \frac{\Delta\nu_{\text{line}}}{\nu} \approx 0.003 \frac{\Delta\nu_{\text{line}}}{100 \text{ MHz}} \frac{30 \text{ GHz}}{\nu} \quad (33)$$

does the periodic structure get effectively smeared out.

We illustrate the effect of a small asymmetry or inertial defect on the distribution of lines in Fig. 1 and on the resulting observed spectrum in Fig. 2.

To summarise, this analysis shows that for an asymmetry ϵ less than a few percent and a dimensionless inertial defect δ less than a few times 10^{-4} , the rotational spectrum conserves the appearance of a “comb” when observed with a few MHz resolution. Higher asymmetries rapidly lead to an unusable quasi-continuum spectrum, whereas higher inertial defects (up to a few times 10^{-3}) lead to the broadening of the “teeth” but still conserve the periodicity of the pattern. We show explicitly in Appendix A that for ϵ, δ less than these critical values, the comb “teeth” are not only evenly spaced, they fall precisely (within an error much smaller than a few MHz) at frequencies

$$\nu_J = \Delta\nu_{\text{line}} \left(J + \frac{1}{2} \right), \quad (34)$$

where J is an integer and $\Delta\nu_{\text{line}} = 2A_3(1 + \mathcal{O}(\epsilon^2, \delta))$. This very simple pattern will make it possible to use simple matched-filtering techniques to look for PAH rotational lines (see Section 4).

We now turn to estimating the level of asymmetry and inertial defect of realistic PAHs.

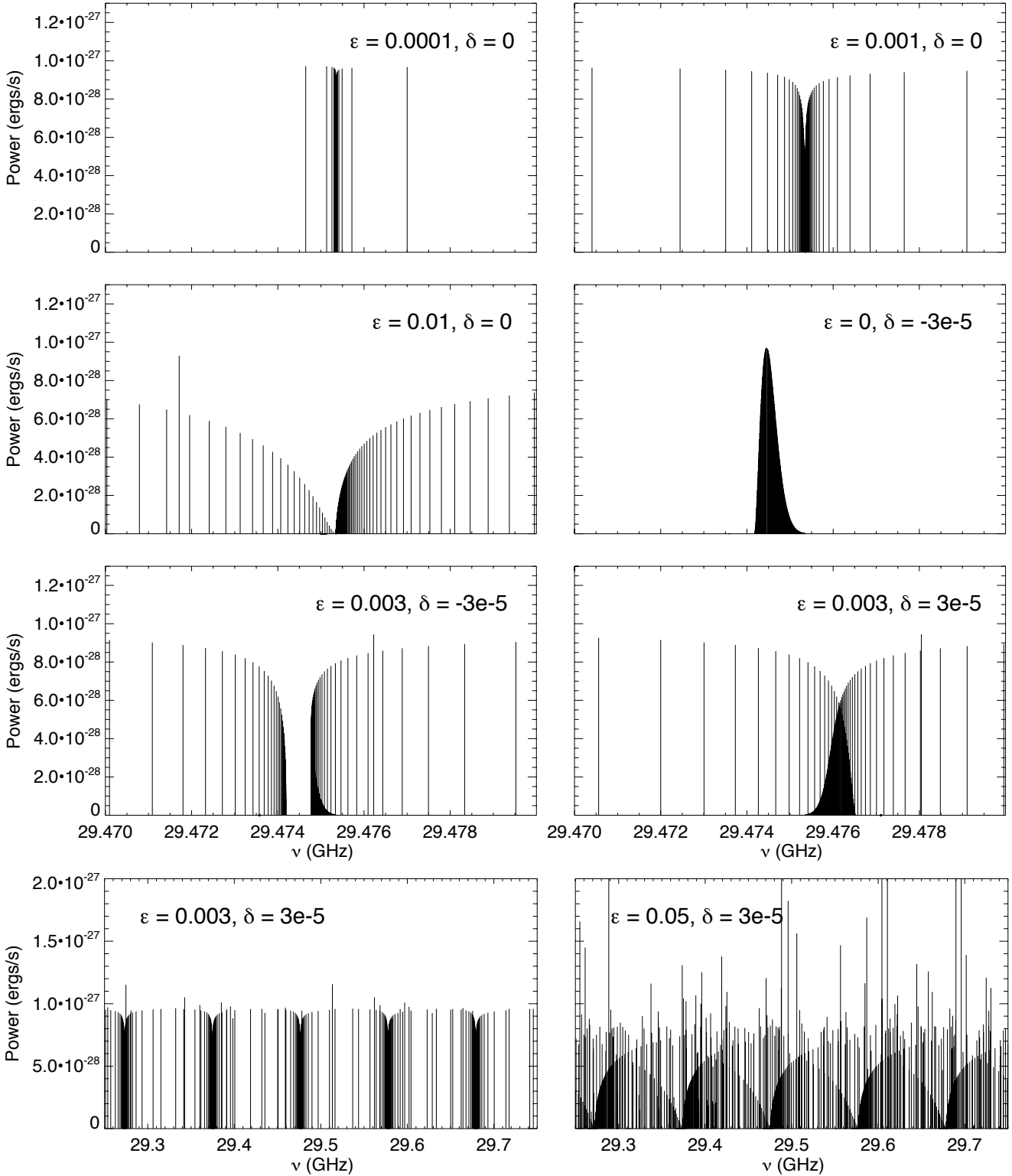


Figure 1. Effect of a small asymmetry ϵ and a small inertial defect δ on the rotational spectrum of a nearly symmetric planar PAH of about 40 carbon atoms (corresponding to a line spacing of about 100 MHz), with dipole moment $\mu_{\text{ip}} = 2$ Debye. The probability distribution for the rotation state was set to $P(J) \propto J^2 \exp[-(J/90)^2]$ and the distribution $P(K|J)$ was conservatively assumed to be uniform (this is a physically motivated assumption, see for example Silsbee et al. 2011; it is conservative because a distribution more sharply peaked around $K = J$ would lead to less spread in the lines). With this distribution function, the rotational emission peaks around 30 GHz. The top 6 panels show the detail of clustering of the $\Delta J = -1, \Delta K = -1$ transitions with constant $2J - K$ over a 10 MHz region. For a perfectly symmetric grain with no inertial defect all the lines would be stacked at the same frequency. The bottom two panels show the line intensity over a 500 MHz region. For a small asymmetry ($\epsilon = 0.003$), lines accumulate at evenly spaced frequencies, whereas for a relatively large asymmetry ($\epsilon = 0.05$), the spectrum becomes a dense forest of lines.

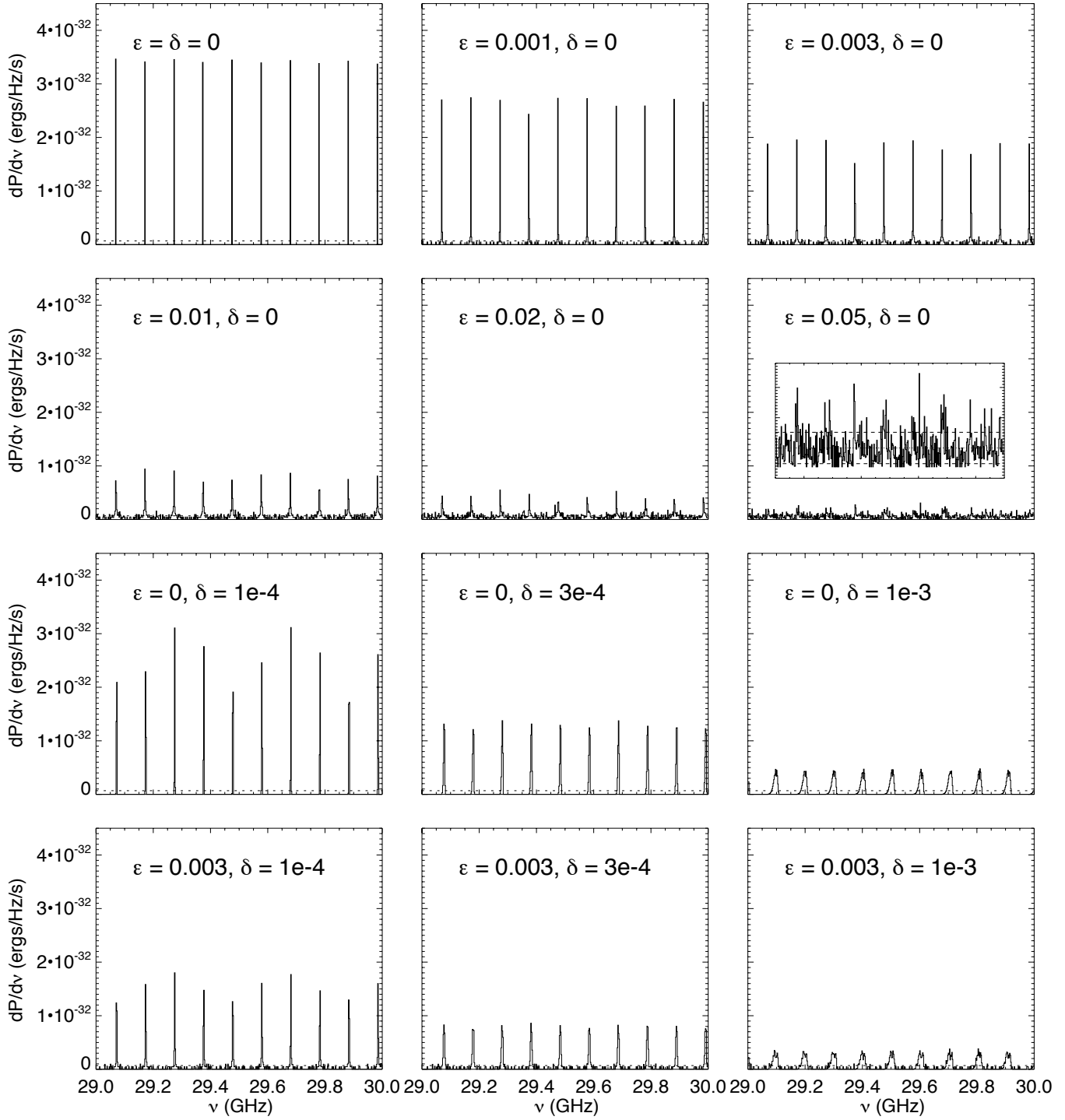


Figure 2. Appearance of the rotational spectrum of a PAH with line spacing of about 100 MHz observed with a resolution $\Delta\nu_{\text{res}} = 2$ MHz, for several values of the asymmetry parameter and inertial defect. The dotted lines denote the mean. Negative inertial defects produce the same qualitative behaviour. The inset in the spectrum for $\epsilon = 0.05, \delta = 0$ has a smaller y -scale and shows that for such a level of asymmetry the line intensity is comparable to the intrinsic variance of the spectrum (the dotted line denotes the mean and the dashed lines denote the $1\text{-}\sigma$ rms fluctuation about the mean).

3 EXPECTED IMPERFECTIONS OF REALISTIC PAHS

3.1 Characteristic magnitude of the inertial defect

It is in principle possible to compute the inertial defect $\Delta \equiv I_3 - I_1 - I_2$ of a symmetric molecule from first principles, see Jagod & Oka (1990) and references therein. The inertial defects of a few small PAHs have been either measured or computed (see for example Thorwirth et al. 2007); however, for large PAHs such computations become very involved, and to our knowledge no experimental nor theoretical values are currently available.

Based on measured inertial defects for a few small aromatic molecules, Oka (1995) provides a fit to the inertial defect in the ground vibrational state, as a function of the wavelength of the lowest-lying vibrational mode λ_0 and of the largest moment of inertia I_3 :

$$\frac{\Delta}{1 \text{ amu } \text{Å}^2} \approx -0.34 \frac{\lambda_0}{100 \text{ } \mu\text{m}} + 0.80 \left(\frac{I_3}{10^4 \text{ amu } \text{Å}^2} \right)^{1/2}. \quad (35)$$

The first, negative term comes from the the small non-planarity induced by out-of plane zero-point vibrations. The second, positive term does not have a simple classical analog and arises from vibration-rotation interactions.

Based on the computed rotational constants of coronene and circumcoronene (Hudgins et al. 2005), we obtain the following scaling for the principal moment of inertia for disc-like PAHs:

$$I_3 \approx 1.5 \times 10^4 \left(\frac{N_C}{54} \right)^2 \text{ amu } \text{Å}^2. \quad (36)$$

The lowest-lying vibrational mode of coronene is at $\lambda_0 \approx 80 \text{ } \mu\text{m}$, and that of circumcoronene is at $\lambda_0 \approx 180 \text{ } \mu\text{m}$ (Bauschlicher et al. 2010; Boersma et al. 2011). Using Eq. (36), equation (35) gives inertial defects $\Delta \approx 0.2$ and $0.4 \text{ amu } \text{Å}^2$ for coronene and circumcoronene, respectively. These values are certainly highly inaccurate, but one may expect the inertial defect to be of order a few tenths of $\text{amu } \text{Å}^2$, except for molecules with unusually low vibrational frequencies or unusually low rigidity. For reference, the measured inertial defect of the symmetrical benzene molecule C_6H_6 is $0.05 \text{ amu } \text{Å}^2$ (Jagod & Oka 1990). On the other hand the following asymmetric molecules have a negative inertial defect: that of azulene C_{10}H_8 is $-0.15 \text{ amu } \text{Å}^2$, that of acenaphthylene C_{12}H_8 is $-0.19 \text{ amu } \text{Å}^2$ (Thorwirth et al. 2007) and that of pyrene $\text{C}_{16}\text{H}_{10}$ is $-0.6 \text{ amu } \text{Å}^2$ (Baba et al. 2009).

Using Eq. (36), the dimensionless inertial defect is of order

$$\delta \approx 3 \times 10^{-5} \left(\frac{54}{N_C} \right) \frac{\Delta}{0.4(N_C/54) \text{ amu } \text{Å}^2}, \quad (37)$$

where we have normalised the inertial defect to a scaling law fitting approximately the measured value for benzene and the estimates we obtained for coronene and circumcoronene.

We conclude that as long as the inertial defect does not exceed expected values of a few tenths of $\text{amu } \text{Å}^2$ for PAHs with $N_C \sim 50$, its effect on the rotational spectrum is negligible or at most minor, with $\delta \lesssim 10^{-4}$. Accurate computations of the inertial defect of large PAHs in order to confirm this statement would be highly valuable.

3.2 Degree of asymmetry of symmetric PAHs with imperfections

Let us first consider a simplified model for a compact, symmetric PAH, which we model as a constant surface-density disc. Assuming a C-C bond length of 1.4 Å , Circumcoronene $\text{C}_{54}\text{H}_{18}$ can be modelled as a disc of radius $a \approx 6 \text{ Å}$, having a mass $M \approx 666 \text{ amu}$, this corresponds to a surface density $\sigma = M/(\pi a^2) \approx 10^{-7} \text{ g/cm}^2$, leading to unperturbed moments of inertia $I_3 = 2I_1 = 2I_2 = \frac{\pi}{2} \sigma a^4 = \frac{1}{2} M a^2$.

Let us now assume that we place an impurity of mass δm at a distance d from the centre of mass. The principal axis of lowest inertia passes through the centre of mass and the impurity (we call this axis 1), and the second axis is perpendicular to it. The displacement of the centre of mass leads to a small change in the moment of inertia quadratic in $\delta m/M$. Neglecting this small term, the moment of inertia I_1 is unchanged with the addition of the mass, whereas I_2 is perturbed by an amount $\delta I_2 = \delta m \times d^2$. The asymmetry parameter is therefore, to lowest order (using $A_1 \approx A_2 \approx 2A_3$)

$$\epsilon = \frac{A_1 - A_2}{2A_3} = 2 \frac{\delta I_2}{I_3} = 4 \frac{d^2 \delta m}{a^2 M}. \quad (38)$$

With $M \approx 12 m_p N_C$, where m_p is the proton mass and N_C is the number of carbon atoms, and $N_C \approx 54(a/6\text{Å})^2$, we find

$$\epsilon \approx 6 \times 10^{-4} \left(\frac{N_C}{54} \right)^{-2} \frac{\delta m}{2m_p} \left(\frac{d}{1.4 \text{ Å}} \right)^2. \quad (39)$$

We have implemented a more realistic PAH model with a honeycomb skeleton, setting the C-C bond length to 1.4 Å and the C-H bond length to 1.1 Å , and found that Eq. (39) gives an accurate estimate of the asymmetry parameter.

We see right away that substituting a peripheral hydrogen by a radical such as CH_3 or adding a benzene ring to the periphery of a symmetric PAH would lead to an asymmetry of at least several percent and therefore wash out the comb emission. Only relatively minor changes (δm of a few m_p) would preserve a sufficient degree of symmetry. We now examine what kind of imperfections may lead to an electric dipole moment, yet preserve a well-identifiable comb spectrum.

3.2.1 Nitrogen substitution

Based on the observed position of the $6.2 \text{ } \mu\text{m}$ feature, Hudgins et al. (2005) argued that nitrogen-substituted PAHs could represent a significant fraction of the PAH population, and estimated the N/C substitution rate in PAHs to be of at least 3%. Note that this number is uncertain: for example Pino et al. (2008) have argued that the shift in the $6.2 \text{ } \mu\text{m}$ feature can also be explained by the presence of aliphatic bonds. Keeping this caveat in mind, we shall assume a fiducial N/C substitution rate of 3% in what follows. Nitrogen-substituted PAHs are strongly polar, with dipole moments of a few Debyes (see Table 5 of Hudgins et al. 2005), and, according to Eq. (39), remain symmetric enough to produce sharp combs of lines.

With a substitution rate of 3%, about 1/3 of coronene and circumcoronene are singly-substituted. There are 3 and 6 distinct possibilities of N-coronenes and N-circumcoronenes, respectively (see Fig. 2 of Hudgins et al.

Table 2. Properties of singly nitrogen substituted coronene and circumcoronene. The numbering of substitution positions corresponds to that shown in Table 1. The dipole moment is obtained from Hudgins et al. 2005. The asymmetry parameter is approximate and estimated assuming a fixed honeycomb carbon skeleton with 1.4 Å C-C bonds and 1.1 Å C-H bonds. The fractional abundance is with respect to the total amount of singly-substituted coronene (or circumcoronene) made entirely of C¹² and in a given charge state.

N-Coronene		(NC ₂₃ H ₁₂)	
Position	μ (Debye)	Asymmetry ϵ	Fraction
1	2.67	0.003	1/4
2	3.69	0.010	1/4
3	5.48	0.018	1/2
N-Circumcoronene		(NC ₅₃ H ₁₈)	
Position	μ (Debye)	Asymmetry ϵ	Fraction
1	1.32	0.0005	1/9
2	4.55	0.0021	1/9
3	5.43	0.0036	2/9
4	6.79	0.0067	1/9
5	6.99	0.0083	2/9
6	9.23	0.0100	2/9

2005 and Table 1 of this paper), some with twice the abundance of others due to a larger phase-space. The number of distinct isomers grows rapidly with the number of substitutions: there are 29 unequivalent doubly-substituted coronene “isomers”, and over 100 kinds of doubly-substituted circumcoronene. Even if these species tend to have a larger dipole moment (though it may also vanish if the two nitrogens are substituted at symmetric locations), they tend, firstly, to have a larger asymmetry parameter. Secondly, and more importantly, the large number of different “isomers” dilutes the power that is radiated in any single comb. The rotational emission of multiply-substituted PAHs therefore add up to a quasi-continuum, whereas singly-substituted molecules produce isolated combs. The latter represent our best candidate for a detection. We show the dipole moments computed by Hudgins et al. (2005) and our estimated asymmetry parameters for singly-substituted coronene and circumcoronene in Table 2.

3.2.2 Dehydrogenation / super-hydrogenation

Under the harsh ISM conditions, small PAHs may lose several, and up to all of their peripheral hydrogen atoms. Le Page et al. (2003) found that PAHs with $\sim 20 - 30$ carbon atoms are typically stripped of most of the peripheral hydrogens (often all of them), whereas larger PAHs typically have normal hydrogen coverage, the transition being a sharp function of size. As long as peripheral hydrogen atoms are either completely stripped off or all in place, the resulting molecule remains symmetric and non-polar. If one peripheral hydrogen is missing, or if there is only one H present, or if there is one additional H on top of a full coverage, the PAH acquires a permanent dipole moment as well as a small asymmetry. The loss or addition of more than one hydrogen atom leads to a large number of sub-families among which the power in

rotational lines is spread. Given the sharp transition from full-hydrogenation to full-dehydrogenation, it is likely that the species that could be of interest, namely singly (de- or super-) hydrogenated PAHs represent a small fraction only of the total PAH abundance. We shall make the optimistic assumption that nitrogen-substituted PAHs are mostly either fully hydrogenated or completely dehydrogenated.

3.2.3 ¹³C substitution

The interstellar ¹²C/¹³C ratio is approximately 70 (see Ritchey et al. 2011 and references therein). Assuming the isotopic ratio is the same among PAH carbon atoms, this implies that $\sim 30\%$ of coronene and $\sim 55\%$ of circumcoronene contain one ¹³C atom or more. ¹³C-substitution by itself does not lead to any significant dipole moment: if the substitution is at a distance d from the centre of a symmetric PAH of mass M , the centre of mass is displaced by $\sim (m_p/M)d$ with respect to the centre of charge, which implies a dipole moment of a few 10^{-3} Debyes at most for a PAH of ~ 50 carbon atoms. However, ¹³C substitution does change the rotational constant of the bearing PAH. Polar nitrogen-substituted PAHs which in addition have one or more ¹³C in their skeleton therefore get subdivided in a large number of sub-families, depending on the relative position of the N and ¹³C atoms in the skeleton, each with different rotational constants and spectrum. They therefore contribute to the quasi-continuum spinning dust emission. Only nitrogen-substituted PAHs that are made purely of ¹²C are susceptible of having strong combs, that is, $\sim 70\%$ of coronene and $\sim 45\%$ of circumcoronene.

3.2.4 Deuterium substitution

The measured D/H ratio varies significantly from one sightline to another, from about ~ 7 ppm to values closer to the primordial ratio of ~ 26 ppm (Linsky et al. 2006). Astration alone cannot easily explain such variations, due to the lack of correlation with variation in the O/H ratio, and Draine (2006) suggested that deuterated PAHs may contain a significant fraction of the interstellar deuterium. Measurements of the weak 4.65 μm feature characteristic of the C-D stretching mode in deuterated PAHs indeed indicate that the D/H ratio in PAHs could be as high as ~ 0.3 (Peeters et al. 2004). If this is the case, all PAHs will have at least a few deuterium atoms in their periphery, resulting in a large number of families with different rotational constants, and diluting all combs into a quasi-continuum. This hypothesis remains to be firmly confirmed, however, and in any case not all sightlines show a low D/H ratio, so one can expect that in some cases PAHs are mostly deuterium-free. We will make this assumption but keep in mind that deuterium-substitutions may very well significantly dilute our predicted signal.

3.2.5 Charge states

Different charge states should have slightly different rotational constants. Even a relative difference of 10^{-4} would lead to a shift of lines by a few MHz at a few tens of GHz. Each N-PAH is therefore divided among several charge states with a priori different rotational constants. Luckily,

small PAHs are found mostly in two states (see for example Fig. 1 of Draine & Lazarian 1998b), i.e. this implies a reduction of each comb strength by a factor of ~ 2 only.

3.3 Conclusion of this section

Let us summarise the essential conclusions of this section:

- The spectrum of an ideal planar and highly symmetrical PAHs with D_{6h} or D_{3h} symmetry would appear as a perfect “comb” of line stacks, each one being made of a large number of lines sharing the same frequency.

- A small asymmetry or inertial defect breaks the frequency degeneracy and spread the radiated power of each stack over a finite frequency interval. Provided these defects are small enough, each stack may still appear as a strong “line” when observed with a few MHz resolution. Inertial defects no larger than several tenths of $\text{amu } \text{\AA}^2$ and asymmetries of a percent or less are small enough to preserve the comb structure of the observed spectrum.

- The majority of any PAH “family” (such as coronene and all substituted versions of it) is divided into a very large number of different “isomers” with different rotational constants. These isomers may be quite symmetric and each emit a comb of lines, but in general the abundance in any one of them is small so their combined rotational emission makes up a quasi-continuum unusable for the purposes of identification.

- A few special isomers are at the same time highly polar, highly symmetric, and over-abundant: these are the singly nitrogen-substituted PAHs, made exclusively of C^{12} , and not suffering from any other defect such as deuterium substitution or dehydrogenation. Assuming the latter two defects are rare (and keeping in mind that their actual rate of occurrence is very uncertain), the largest fraction of coronene in a single “isomer” is $\sim 0.7 \times 0.5 \times 0.36 \times \frac{1}{2} \approx 6\%$, where the factors are the fraction of pure- C^{12} coronene, the fraction in each of the two main charge states, the fraction of single nitrogen-substitution, and the fraction of those in the most abundant isomer. These fractions decrease with size and the corresponding number for circumcoronene is $\sim 0.45 \times 0.5 \times 0.32 \times \frac{2}{9} \approx 1.6\%$. For PAHs with D_{3h} symmetry (the approximately triangle-shaped PAHs in Table 1) instead of D_{6h} symmetry (the approximately hexagon-shaped PAHs, such as coronene and circumcoronene), the number of “isomers” is about twice as large, and this fraction is twice as small.

4 SEARCHING FOR COMBS IN THE SPINNING DUST FOREST

The idea to search for the rotational emission of specific symmetric top PAHs has already been suggested by Lovas et al. (2005), and a search for corannulene $C_{20}H_{10}$ has been carried by Pilleri et al. (2009) in the Red Rectangle, who set an upper limit $N_{C_{20}H_{10}}/N_H < 3 \times 10^{-11}$ by targeting the specific $J = 135 \rightarrow 134$ transition at 137.615 GHz.

Looking for a single line, however, is suboptimal, as the peculiarity of rotation spectra of a planar symmetric top, is that the rotational lines fall almost exactly at positions $\nu = (J + 1/2)\Delta\nu_{\text{line}}$. The purpose of the last section was to demonstrate that for small enough asymmetry and inertial

defect, this pattern is preserved, and that singly nitrogen-substituted PAHs do satisfy these requirements.

Rather than searching for a specific line, a better search strategy is to use the largest possible bandwidth with the best possible resolution, and search for *comb patterns*, resulting in a much enhanced signal-to-noise ratio (by a factor of the square root of the number of lines observable within the total bandwidth). This has the additional advantage of allowing for a blind search over a large range of values of $\Delta\nu_{\text{line}}$, hence over a broad range of carrying species, rather than focusing on a single species at a time.

In what follows we illustrate a simple method to extract a comb signal from a noisy spectrum, identical in spirit to matched-filtering methods used for the search of gravitational wave signals. We consider N_{bins} flux measurements d_i at frequencies ν_i , with constant resolution $\Delta\nu_{\text{res}}$, and over a total bandwidth $\Delta\nu_{\text{tot}} = N_{\text{bins}}\Delta\nu_{\text{res}}$. We assume that we have subtracted the broadband average from the signal, obtained for example by averaging the data over 1 GHz bands. The measured signal is noisy, with a noise n_i , which we assume to be uncorrelated with a known variance: $\overline{n_i n_j} = \mathcal{N}^2 \delta_{ij}$. The derivation below can be easily generalised to frequency-dependent and correlated noise using the noise covariance matrix.

Let us assume that the signal contains N_{combs} combs (labelled with subscripts a, b) with respective line spacings $\Delta\nu_{\text{line}}(a) = \Delta\nu_a$, and peak flux density s_i^a (where we have again subtracted the broadband average from the flux in the combs), so the data can be written as

$$d_i = n_i + \sum_a s_i^a. \quad (40)$$

For two functions f, g with zero mean, we define the scalar product

$$\langle f \cdot g \rangle \equiv \frac{1}{N_{\text{bins}}} \sum_{i=1}^{N_{\text{bins}}} f_i g_i, \quad (41)$$

which is just the average of their product over the observed bandwidth, and the associated norm $\|f\| \equiv \langle f^2 \rangle^{1/2}$. Providing the bandwidth is no more than a few GHz, the amplitude associated with each comb should be approximately constant across the observed frequency range. The underlying signal can therefore be decomposed onto the infinite set of dimensionless “comb” basis functions $c_i^a \equiv c_i(\Delta\nu_a)$, which are unity in frequency bins containing a line and zero otherwise, minus the resulting mean (i.e. $c_i^a \approx 1 - \frac{\Delta\nu_{\text{res}}}{\Delta\nu_a}$ if there exists an integer J such that $\nu_i - \Delta\nu_{\text{res}}/2 < (J + 1/2)\Delta\nu_a < \nu_i + \Delta\nu_{\text{res}}/2$ and $-\frac{\Delta\nu_{\text{res}}}{\Delta\nu_a}$ otherwise). We show an example in Fig. 3 for clarity. The signal can therefore be approximately rewritten as

$$s_i^a \approx \mathcal{A}_a c_i^a, \quad (42)$$

where \mathcal{A}_a is the peak flux density. The comb basis functions are nearly orthogonal for the scalar product (41): if two spacings $\Delta\nu_a$ and $\Delta\nu_b$ are not harmonics of one another, the scalar product $\langle c^a \cdot c^b \rangle$ is typically much smaller than $\|c^a\| \times \|c^b\|$. It is not in general exactly zero because of the finite bandwidth, but is *on average* zero (when keeping $\Delta\nu_a$ fixed and varying $\Delta\nu_b$ for example), and has a variance

$$\overline{\langle c^a \cdot c^b \rangle^2} = \frac{\|c^a\|^2 \|c^b\|^2}{N_{\text{bins}}} \ll \|c^a\|^2 \|c^b\|^2, \quad \text{if } a \neq b. \quad (43)$$

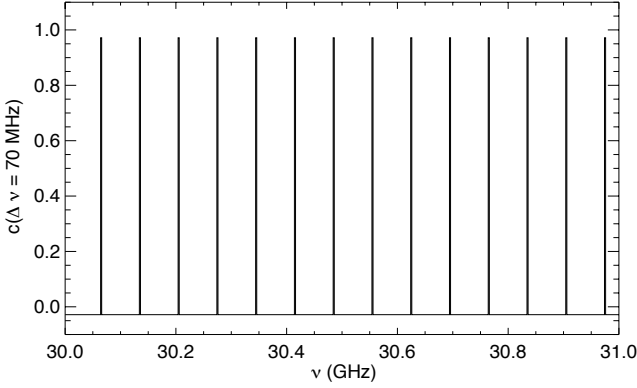


Figure 3. Dimensionless comb basis function $c(\Delta\nu = 70 \text{ MHz})$, for frequency bins $\Delta\nu_{\text{res}} = 2 \text{ MHz}$. The base is offset from zero because we have subtracted the mean.

The norm of each comb basis function is

$$\|c^b\|^2 \approx \frac{N_{\text{lines}}^b}{N_{\text{bins}}} = \frac{\Delta\nu_{\text{tot}}}{\Delta\nu_b}, \quad (44)$$

where $N_{\text{lines}}^b \equiv \frac{\Delta\nu_{\text{tot}}}{\Delta\nu_b}$ is the number of lines of the comb b within the full bandwidth.

The matched-filtering consists in computing the following quantity as a function of comb spacing:

$$\mathcal{S}(\Delta\nu_b) \equiv \frac{\langle d \cdot c^b \rangle}{\|c^b\|^2} = \frac{\langle n \cdot c^b \rangle}{\|c^b\|^2} + \sum_a \mathcal{A}_a \frac{\langle c^a \cdot c^b \rangle}{\|c^b\|^2}. \quad (45)$$

The mean of \mathcal{S} is the amplitude of the comb signal with spacing $\Delta\nu_b$, providing such a comb exists in the data³,

$$\langle \mathcal{S}(\Delta\nu_b) \rangle = \mathcal{A}_b, \quad (46)$$

and its variance in the absence of signal at $\Delta\nu_b$ is the sum of the instrumental noise and the contribution from the signal itself:

$$\langle \delta \mathcal{S}^2 \rangle = \frac{1}{N_{\text{bins}} \|c^b\|^2} \left[\mathcal{N}^2 + \sum_a \|s^a\|^2 \right] = \frac{\|d\|^2}{N_{\text{lines}}^b}, \quad (47)$$

where $\|d\|$ is just the rms fluctuation of the total data (signal and noise). The signal-to-noise ratio (hereafter, SNR) is therefore

$$\text{SNR}(\Delta\nu_b) = \frac{\langle \mathcal{S}(\Delta\nu_b) \rangle}{\langle \delta \mathcal{S}^2 \rangle^{1/2}} = \frac{\sqrt{N_{\text{lines}}^b} \mathcal{A}_b}{\langle d^2 \rangle^{1/2}}, \quad (48)$$

i.e. it is enhanced by a factor of $\sqrt{N_{\text{lines}}^b}$ with respect to the single-line signal-to-noise ratio. For a bandwidth of order 10 GHz and a line spacing of order 100 MHz, this enhancement is a factor of 10.

Since the noise per bin is $\mathcal{N} \propto 1/\sqrt{\Delta\nu_{\text{res}}}$ (and similarly

³ We have ignored the fact that $\mathcal{S}(\Delta\nu_b)$ is also non-zero if the signal contains harmonics of $\Delta\nu_b$. We have found that the dominant harmonics are combs with 3, 1/3, 5 and 1/5 times the fundamental spacing, with contributions a factor of a few smaller than that of the principal value. One could account for this fact (and utilise it to extract more information) with a more sophisticated data analysis technique, but this is beyond the scope of the present work, and we shall neglect resonances for simplicity.

for $\|d\|$) and the flux density in each line is inversely proportional to the bin width, $\mathcal{A} \propto 1/\Delta\nu_{\text{res}}$, we see that the signal-to-noise ratio increases proportionally to $\sqrt{\Delta\nu_{\text{tot}}/\Delta\nu_{\text{res}}}$. Even if the noise level increase when increasing the resolution, the line intensity increases faster. It is therefore best to have as large a bandwidth as possible and as high a resolution as possible. In practice, however, there is no point in having a resolution better than the turbulent velocity broadening, of magnitude $\Delta\nu_{\text{turb}} = 1 \text{ MHz} \times (v_{\text{turb}}/10 \text{ km/s})$ at 30 GHz.

We illustrate the method in Figs. 4 and 5. We have simulated the rotational spectrum of a ~ 40 -carbon atom planar PAH, with rotational constant $A_3 \approx 50 \text{ MHz}$, asymmetry parameter $\epsilon = 3 \times 10^{-3}$, no inertial defect, and permanent dipole moment $\mu = 2 \text{ Debye}$. We assumed a probability distribution $P(J, K) \propto J \exp[-(J/90)^2]$, so the spectrum peaks near 30 GHz. We convolved the spectrum with a 2 MHz window function over a 10 GHz bandwidth (Fig. 4, right panel), and added a gaussian random noise with a rms value of slightly more than a third of the mean line amplitude (Fig. 4, left panel). With this configuration, no individual line could have been detected at the 3- σ level. We performed a blind search over comb spacings $\Delta\nu$, as described above. The SNR as a function of $\Delta\nu$ is shown in Fig. 5. We see that in this case the input comb is detected with a very high SNR (about 25 in this example), and the line spacing is recovered with very high accuracy.

Let us finally point out that there is an intrinsic “noise” to the signal originating in its non-smoothness, represented by the $\sum_a \|s^a\|^2$ term in Eq. (47). If there are too many combs with comparable amplitudes, the signal may indeed disappear under the grass. For N_{comb} combs with similar amplitude, the “noise” due to the lines themselves is $(\sum_a \|s^a\|^2)^{1/2} \approx \sqrt{N_{\text{comb}}} \mathcal{A} \sqrt{N_{\text{lines}}^b/N_{\text{bins}}}$, which would become comparable to $\sqrt{N_{\text{lines}}^b} \mathcal{A}$ if $N_{\text{comb}} \sim N_{\text{bins}}$, i.e., for a bandwidth of several GHz and a few MHz resolution, if there are more than ~ 1000 species with comparable abundance emitting sharp comb signals. While this seems unlikely, should this be the case, if the intrinsic “noise” due to the PAH combs is significantly larger than the instrumental noise, one should still be able to detect the presence of small PAHs from the anomalous noise level. This would require an accurate calibration of the instrumental and atmospheric noise by switching regularly to a relatively empty field of view with no expected PAH emission. Whereas this is in principle possible, the practical implementation of such a search is likely to be challenging, and so would be the interpretation of the results. We have therefore not analysed this option in more detail in this paper.

5 DETECTION FORECASTS

5.1 Expected SNR from the observed spinning dust emission

One can in principle predict the intensity of the rotational lines of any given PAH given the local environment (density, temperature, ambient radiation field, etc...). The first step is to compute the distribution $P(J, K)$ for the angular momentum and configuration of the grain (see for example Ali-Haïmoud 2013 for a review of the theory). The spectrum

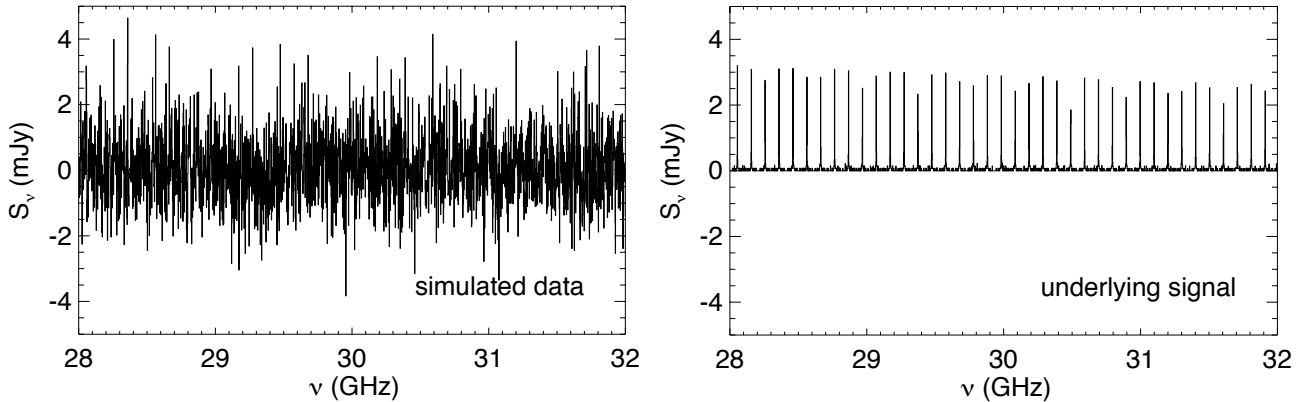


Figure 4. Simulated data, normalised to the rms noise value, assumed uniform across the full bandwidth. Observations are over a 10 GHz total bandwidth (only 4 GHz are shown for better clarity), with a 2 MHz resolution. The assumed underlying signal is shown in the right panel, and was computed assuming a rotational constant $2A_3 = 101.46$ MHz (corresponding to $N_C \sim 40$), an asymmetry $\epsilon = 3 \times 10^{-3}$, no inertial defect, a dipole moment $\mu = 2$ Debye, and a Maxwellian distribution for J such that the emission peaks around 30 GHz.

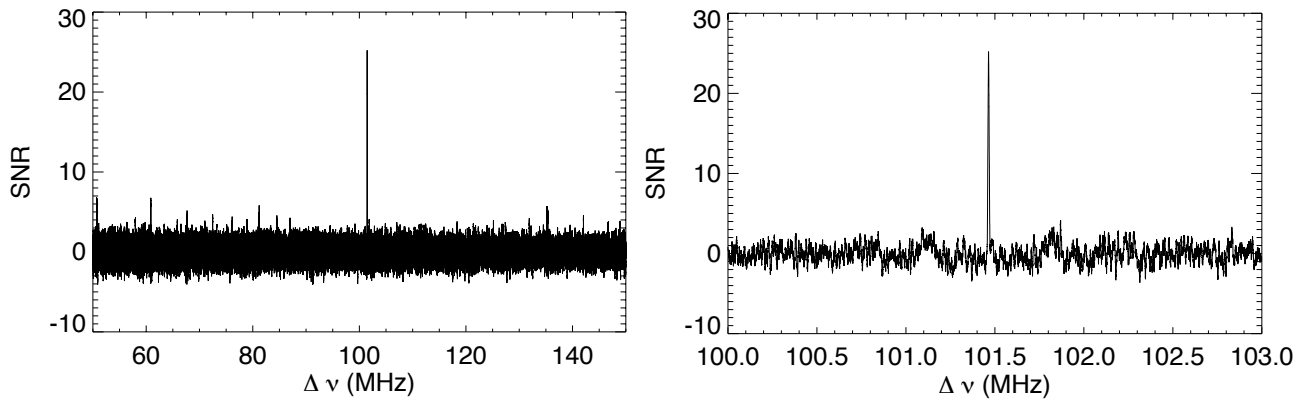


Figure 5. Signal-to-noise ratio obtained with the matched-filtering technique described in this Section, as a function of trial line spacing $\Delta\nu$, and using the data shown in Fig. 4. The right panel is a zoom near the $\Delta\nu \approx 100$ MHz region. The matched-filtering technique allows to detect the underlying comb with SNR of 25, and to recover the input frequency with very high accuracy.

is then readily obtained given the asymmetry parameter and inertial defect, using Eqs. (24)-(26) for the power radiated in each line, for which the exact frequency is easily computed from the expression for the energy levels (23). Code to do these computations using output from SPDUST (Ali-Haïmoud et al. 2009) can be obtained from the author.

It is however difficult to estimate the exact conditions along a given line of sight (and these conditions are more-over non-uniform), and we have chosen instead in this work to estimate the rotational line intensity from the observed anomalous microwave emission (hereafter, AME). The latter is indeed believed to be due to spinning dust radiation which is the broadband equivalent of the rotational line emission we are searching for.

The first step is to relate the line intensity of any given specific PAH “isomer” (such as neutral $\text{NC}_{23}\text{H}_{12}$ with nitrogen in the innermost ring) to the overall broadband emission from all its “family” (continuing with our previous example, all the substituted versions of coronene, including multiple nitrogen substitutions, isotope substitutions, and different charge states). The intensity of combs produced by each isomer decreases with increasing asymmetry and depends on the dipole moment μ in two ways: first, the power radi-

ated is proportional to μ^2 , second, the characteristic rotation rate hence the peak of the emission decreases with increasing dipole moment due to the radiation reaction torque, see for example Fig. 12 of Ali-Haïmoud et al. (2009). The dipole moment increases with the asymmetry parameter (see Table 2), and these two quantities have approximately an opposite effect on the line intensity (provided the observation frequency is near the peak of the emission). Guided by this observation, we shall assume that the line intensity is approximately constant among different isomers, and equal to that of the most symmetric isomer. We have currently no observational handle on the characteristic dipole moment of PAHs. Draine & Lazarian (1998b) assume that $\mu \approx 0.4$ Debye $\times \sqrt{N_{\text{atoms}}}$, based on the known dipole moments of a few small carbonaceous and nitrogenated radicals. The reasonable agreement of the Draine & Lazarian (1998b) spinning dust model with observations indicates that this characteristic dipole moment gives, at least within a factor of a few, a relatively accurate representation of real polar PAHs. This simple scaling gives $\mu \approx 2.4$ Debye for coronene and 3.4 Debye for circumcoronene, which is comparable to the dipole moment of their most symmetrical nitrogen-substituted isomers, where the nitrogen atom is in one of the innermost

rings. From these considerations, we shall assume that intensity in the lines of any isomer is comparable to the intensity of a PAH with no asymmetry and with a “typical” dipole moment, i.e. comparable to the rms dipole moment of the PAHs producing the broadband spinning dust emission. We may therefore relate the flux in any line due to a particular isomer to the broadband flux emitted by its entire “family” as

$$S_{\nu}^{\text{line}}(\text{isomer}) \sim \frac{N_{\text{isomer}}}{N_{\text{family}}} \frac{\Delta\nu_{\text{line}}}{\Delta\nu_{\text{res}}} S_{\nu}^{\text{bb}}(\text{family}), \quad (49)$$

where $\Delta\nu_{\text{line}}$ is the line spacing for the PAH considered and S_{ν}^{bb} is the broadband emission resulting from the whole “family” of similar isomers.

The next step is to relate the broadband emission from a single PAH “family” to the total spinning dust emission, S_{ν}^{AME} , which is sourced by all (or at least the smallest) of the PAHs. We denote by $N_{\text{PAH,tot}}$ the total abundance of PAHs responsible for the AME – more precisely, the abundance of PAHs with ~ 50 carbon atoms that would contain the same amount of carbon as the whole radiating PAH population. The range of sizes spanned by the PAHs carrying the AME is relatively limited (see for example Fig. 11 of Ali-Haïmoud et al. 2009), and we may assume that

$$S_{\nu}^{\text{bb}}(\text{family}) \sim \frac{N_{\text{family}}}{N_{\text{PAH,tot}}} S_{\nu}^{\text{AME}}. \quad (50)$$

We therefore arrive at the following simple relation between the intensity in the lines of any specific substituted PAH and the broadband AME:

$$\begin{aligned} S_{\nu}^{\text{line}} &\sim \frac{\Delta\nu_{\text{line}}}{\Delta\nu_{\text{res}}} f_{\text{iso}} \frac{N_{\text{family}}}{N_{\text{PAH,tot}}} S_{\nu}^{\text{AME}} \\ &\sim 0.1 \text{ mJy} \frac{\Delta\nu_{\text{line}}}{100 \text{ MHz}} \frac{1 \text{ MHz}}{\Delta\nu_{\text{res}}} \frac{f_{\text{iso}}}{1\%} \frac{N_{\text{family}}}{0.01 N_{\text{PAH,tot}}} \frac{S_{\nu}^{\text{AME}}}{10 \text{ mJy}}, \end{aligned} \quad (51)$$

where $f_{\text{iso}} \equiv N_{\text{isomer}}/N_{\text{family}}$ is the fraction of PAHs of a given family in a specific isomer, and is typically of order a few percent (see discussion in Section 3.3).

The resulting SNR with our matched-filtering analysis and with noise \mathcal{N} per resolution element would then be

$$\begin{aligned} \text{SNR} &\approx \sqrt{\frac{\Delta\nu_{\text{tot}}}{\Delta\nu_{\text{line}}} \frac{S_{\nu}^{\text{line}}}{\mathcal{N}}} \\ &\sim 10 \sqrt{\frac{\Delta\nu_{\text{tot}}}{10 \text{ GHz}} \frac{1 \text{ MHz}}{\Delta\nu_{\text{res}}} \frac{0.1 \text{ mJy}}{\mathcal{N}}} \\ &\times \sqrt{\frac{\Delta\nu_{\text{line}}}{100 \text{ MHz}} \frac{f_{\text{sym}}}{1\%} \frac{N_{\text{PAH}}}{0.01 N_{\text{PAH,tot}}} \frac{S_{\nu}^{\text{AME}}}{10 \text{ mJy}}}. \end{aligned} \quad (52)$$

One should keep in mind that Equation (53) is simply indicative and probably only accurate within an order of magnitude.

For reference, the Spectrometer backend on the Green Bank Telescope (GBT) can allow for a 3.2 GHz bandwidth, with a sub-MHz resolution (but again, we only require $\Delta\nu_{\text{res}} \gtrsim 1$ MHz as beyond this resolution Doppler broadening is likely to smear the lines anyway). The noise level for the KFPA receiver near 26 GHz is approximately⁴

$$\mathcal{N}^{\text{GBT}} \approx 0.7 \text{ mJy} \sqrt{\frac{1 \text{ MHz}}{\Delta\nu_{\text{res}}} \frac{1 \text{ hour}}{\tau_{\text{obs}}}}, \quad (54)$$

⁴ https://dss.gb.nrao.edu/calculator-ui/war/Calculator_ui.html

and a noise level of ~ 0.1 mJy per 1 MHz resolution element can in principle be achieved after ~ 50 hours of observations. The Very Large Array⁵ (VLA) also allows for a sub-MHz frequency resolution over a large bandwidth (8 GHz in the K band), with a noise level better than (but comparable to) that of the GBT. However, because the VLA is an interferometer, it is not sensitive to power on angular scales larger than λ/D_s , where λ is the observation wavelength and D_s is the shortest separation in the array configuration. In the VLA C or D configurations, the largest angular scale accessible is of order 1 arcmin⁶. It is therefore more appropriate to use the GBT for extended sources whereas the VLA would be more suitable for sources that are known to be compact. Finally, we note that quasi-periodic features in the instrument noise could deteriorate the sensitivity to “combs” compared to that predicted in this idealized analysis. Any such features should be accurately characterized prior to a search for PAH lines.

5.2 Potential targets

Anomalous microwave emission has been detected along several lines of sight, and in very different regions of the ISM. A systematic search for lines should be conducted in known AME regions, as well as in regions showing strong PAH infrared emission. Here we simply point out a couple of particularly bright AME sources:

Observations at 31 GHz with CBI reveal the presence of strong AME in the HII region **RCW175** (Dickinson et al. 2009; Tibbs et al. 2012), with a measured flux of 1 Jy per 4' beam. This corresponds to a flux $S_{\nu}^{\text{AME}} \approx 0.16$ mJy per GBT 0.5' beam if the source is extended, and potentially larger if the source is smaller than the 4' CBI beam. For coronene $\Delta\nu_{\text{line}} \approx 340$ MHz and $f_{\text{iso}} \approx 6\%$ for the most abundant isomer, and using Eq. (53) with $\Delta\nu_{\text{tot}} = 3.2$ GHz, one may hope to detect of order $\sim 0.1\%$ of the total PAH abundance concentrated in the coronene “family” with a SNR of ~ 10 , with ~ 50 hours of observations at the GBT. For circumcoronene, with $\Delta\nu_{\text{line}} \approx 70$ MHz and $f_{\text{iso}} \approx 1.6\%$, the same observation would allow to detect approximately 1% of the total PAH abundance concentrated in the circumcoronene “family” with a SNR of ~ 10 .

The **Perseus molecular cloud**, is a well-known source of AME, observed near 30 GHz with the VSA (Tibbs et al. 2011) and the *Planck* satellite (Planck Collaboration 2011). The peak emission in the 7' VSA beam is 0.2 Jy, corresponding to a minimum of 1 mJy per GBT 0.5' beam. If the AME is truly extended this source is less promising but it is likely that the emission arises from regions more compact than the 7' VSA beam.

The detection forecasts obtained from Eq. (53) may seem somewhat challenging. However, we emphasise again that Eq. (53) is only an order of magnitude estimate. It is conceivable that the comb-carrying PAHs are significantly more polar than the bulk of the AME-emitting PAHs, for example. In addition, when studying the effect of an asymmetry or inertial defect on the spectrum, we have assumed conservatively a completely randomised orientation of the

⁵ <http://www.vla.nrao.edu/>

⁶ <https://science.nrao.edu/facilities/vla/docs/>

PAH with respect to the angular momentum axis (i.e. K uniformly distributed between $-J$ and J), which is equivalent to assuming an infinite internal temperature at constant angular momentum. In practice the internal temperature is finite and the distribution of K -values is somewhat peaked around the lowest energy states $K = \pm J$. This reduces the effect of the asymmetry and inertial defect on the spectrum (in the limit that the grain rotates primarily about its axis of greatest inertia, its spectrum is a perfect comb no matter how asymmetric and non-planar it is), and increases the line intensity with respect to our conservative estimate. Finally, current AME observations have a larger angular resolution than that of the GBT; we based our estimate on the conservative assumption that the emission is extended but the signal may be stronger if the source is in fact compact.

5.3 A note on protoplanetary discs

Infrared emission from PAHs is frequently detected in discs around young stars, in particular Herbig Ae/Be stars, the detection rate being smaller in the lower mass T-Tauri stars (Acke 2011; Kamp 2011). Rafikov (2006) has suggested that PAHs may also be observable through their (continuum) rotational radiation in circumstellar discs, peaking around 30-50 GHz. Such an observation would however be made difficult by the presence of other continuum emission processes, such as the vibrational emission from large dust grains. It would therefore be very interesting to search for rotational lines from PAHs in protoplanetary discs with the method we suggest here. A detection of PAH lines would allow for identification of the precise species present, and, combined with spatial information, could shed light on PAH formation and destruction rates in protoplanetary nebulae. Radio interferometers such as the VLA⁷ are ideally suited for such a search, as they already target protoplanetary discs at tens of GHz to measure dust properties (Pérez et al. 2012).

6 CONCLUSIONS

Rotational spectroscopy is a powerful technique to detect individual molecules in the ISM, but has never been applied to PAHs with the exception of corannulene. The main deterrent in searching for the rotational line emission of PAHs has been the fact that they are a priori large triaxial molecules, for which the radiated power is diluted among a very large number of weak lines, making them very difficult to detect. In this paper we have addressed this issue quantitatively, and argued that the prospects for PAH rotational spectroscopy are brighter than what may have been foreseen.

It is reasonable to expect that some specific highly-symmetric, highly-compact PAHs are over-abundant compared to the bulk of the PAH family. This statement on its own does not solve the problem of triaxiality: PAHs indeed need a permanent dipole moment in order to radiate, and symmetric molecules can only be polar if they carry some impurity, which is bound to break their symmetry. We have therefore computed the rotational emission of quasi-symmetric, planar PAHs. Our result is that for a

sufficiently small degree of asymmetry, the rotational spectrum, *observed with a \sim MHz resolution*, has the appearance of a “comb” of evenly spaced strong lines, similar to the spectrum of a much simpler linear molecule. We have then estimated the degree of asymmetry resulting from various imperfections that are likely in the ISM. We have concluded that nitrogen-substituted PAHs are promising targets for rotational spectroscopy, as they remain very symmetric (if the unsubstituted species is so), are highly polar, and are more-over believed to make a significant fraction of the interstellar PAH population.

We have then pointed out that the very peculiar “comb” pattern of the rotational spectrum of quasi-symmetric planar PAHs allows for the use of matched filtering techniques. This can significantly enhance the effective signal-to-noise ratio, and allow for detection of PAH “combs” hidden in noisy spectra. Moreover, the pattern has a single free parameter (the line spacing, directly related to the carrier’s size) and a blind search over PAHs of different sizes is therefore possible. This is much more efficient than targeting a specific species.

Based on the observed level of anomalous microwave emission (AME) in a few regions, we have made a rough estimate of the fraction of PAHs in a specific species that could be detected. We have estimated, assuming conservatively that the emission is extended, that 50 hours of observations of the HII region RCW175 with the GBT could allow for a $10\text{-}\sigma$ detection of about 0.1% of the PAH population in coronene and all its substitutes, assuming the observed AME there is due to broadband PAH rotational emission (usually referred to as spinning dust radiation).

Since the actual distribution of the PAH population among specific species (in particular the highly symmetric ones that can be targeted) is a complete unknown and may depend on the specific environment, we advocate for a broad search campaign in various regions known to harbour AME and/or PAH infrared features. We also point out that protoplanetary disks are interesting targets for interferometers such as the VLA.

If detected, rotational lines would constitute an unambiguous proof of the existence of free-floating PAHs in the interstellar medium, conclusively closing the remaining debate about the nature of the carriers of the aromatic infrared features. The detection of specific PAHs would also shed light on the formation processes of dust, which the first step in the path to planet formation.

ACKNOWLEDGEMENTS

I would like to particularly thank Bruce Draine for several enlightening conversations and detailed comments on the manuscript. I also thank Kfir Blum and Lyman Page for warm encouragements, Laura Pérez for discussions on observational prospects and circumstellar discs, and Chris Hirata for conversations on quantum chemistry of PAHs. The idea that the discrete rotational line emission from dust grains may have observational consequences was first discussed during the “First Billion Years” workshop organised in August 2010 by the Keck Institute of Space Studies. This work was supported by the NSF grant number AST-0807444 at the Institute for Advanced Study.

⁷ <http://www.vla.nrao.edu/>

APPENDIX A: FREQUENCIES OF THE “TEETH” OF THE COMB SPECTRUM

In this appendix we show that a small asymmetry or inertial defect change the spacing of the “comb” spectrum but do not lead to any measurable offset, i.e. the frequencies of the “teeth” are exactly $\nu_J = (J + 1/2)\Delta\nu_{\text{line}}$, up to corrections much smaller than a few MHz.

We shall assume that the probability distribution for the total angular momentum is of the form

$$\text{Prob}(J) \propto J^2 \exp\left[-\frac{3}{2}\left(\frac{J}{\sigma_J}\right)^2\right], \quad (\text{A1})$$

and that K is uniformly distributed in $[-J, J]$, so $\text{Prob}(J, K) \propto \text{Prob}(J)/J$ for $J \gg 1$. The power radiated in the $\Delta J = \Delta K = -1$ transitions at frequency $\nu_{J,K}$ is then, using Eq. (26).

$$\text{Pow}(J, K) \propto \nu_{J,K}^4 \left(1 + \frac{K}{J}\right)^2 J^{-1} \text{Prob}(J). \quad (\text{A2})$$

Defining $J_0 \equiv 2J - K$ so that $\nu_{J,K} \propto J_0$, we may rewrite this in terms of the variables J, J_0 as

$$\text{Pow}(J, J_0) \propto J_0^4 (3J - J_0)^2 J^{-1} \exp\left[-\frac{3}{2}\left(\frac{J}{\sigma_J}\right)^2\right]. \quad (\text{A3})$$

In this expression, J_0 labels a line “stack” (seen as a single “tooth” with finite resolution) whereas $J \in [J_0/3, J_0]$ labels a specific line within the stack.

The total power per stack is obtained by integrating the above expressions over J . We obtain

$$\text{Pow}(J_0) \propto J_0^6 \int_{1/3}^1 dj \frac{(3j-1)^2}{j} \exp\left[-\frac{3}{2}\left(\frac{J_0}{\sigma_J}\right)^2 j^2\right]. \quad (\text{A4})$$

We find numerically that this expression peaks at $J_{0,\text{peak}} \approx 2.458 \sigma_J$.

Let us now consider a fixed stack J_0 . The density of lines per frequency interval is

$$\rho_{\text{line}}(J, J_0) = \left(\frac{d\nu_{J,K}}{dJ}\right)^{-1} \propto \left(1 + \frac{3}{8} \frac{\epsilon^2}{\delta} \frac{(J_0 - J)^2}{(J_0 - 2J)^4} J^2\right)^{-1}. \quad (\text{A5})$$

• If $\delta < 0$, this density becomes infinite, i.e. lines accumulate near

$$\frac{J_{\text{acc}}}{J_0} = \frac{1}{2} \pm \frac{1}{2\sqrt{1 + 8\sqrt{2}\delta/3\epsilon^2}}, \quad (\text{A6})$$

where there are two physical solutions (corresponding to $J \geq J_0/3$) if $\delta \geq \frac{3}{2}\epsilon^2$ and only one solution otherwise, the one with the + sign. When there are two solutions one of them will in general correspond to a larger radiated power (typically, the + solution, since the spontaneous transition rate of this transition vanishes at $K = -J$ and increases towards $K = +J$). Plugging this value back into Eq. (27), we see that lines of the J_0 -th stack accumulate near the frequency

$$\nu_{\text{acc}}(J_0) = A_3 [(2J_0 + 1) + 2J_0 (\epsilon^2 f(\delta/\epsilon^2) + \delta g(\delta/\epsilon^2))], \quad (\text{A7})$$

where f and g are some functions of order unity. We may rewrite this as

$$\nu_{\text{acc}}(J_0) = \tilde{A}_3(2J_0 + 1) + \mathcal{O}(\epsilon^2, \delta)A_3, \quad (\text{A8})$$

where

$$\tilde{A}_3 \equiv A_3 [1 + \epsilon^2 f(\delta/\epsilon^2) + \delta g(\delta/\epsilon^2)]. \quad (\text{A9})$$

For $2A_3 \sim 100$ MHz and $\epsilon^2 \sim \delta \sim 10^{-4}$, the correction term in Eq. (A8) is of order $\sim 10^{-2}$ MHz, much smaller than a resolution bin and is therefore unobservable.

• If $\delta > 0$ lines do not accumulate near any particular frequency, but the radiated power is maximised near some frequency corresponding to J_{max} . In order to find it, we must maximise $\text{Pow}(J, J_0)\rho_{\text{line}}(J, J_0)$ at fixed J_0 . The result is a function of the form

$$J_{\text{max}} = J_0 \mathcal{F}(J_0/J_{0,\text{peak}}, \epsilon^2/\delta). \quad (\text{A10})$$

We solve for \mathcal{F} numerically and find that it is a relatively slowly varying function of J_0 near $J_{0,\text{peak}}$: it varies by at most $\sim 10\%$ for J_0 within $\pm 15\%$ of $J_{0,\text{peak}}$, when ϵ^2/δ spans all real numbers. For reference its value at $J_{0,\text{peak}}$ is $\mathcal{F} \approx 0.5$ for $\epsilon^2 \ll \delta$ to $\mathcal{F} \approx 1$ (independent of J_0) for $\epsilon^2 \gg \delta$.

This implies that the peak frequency within a stack is of the form

$$\begin{aligned} \nu_{\text{peak}} &= A_3 [(2J_0 + 1) + 2J_0 (\epsilon^2 f(\delta/\epsilon^2) + \delta g(\delta/\epsilon^2))] \\ &+ \mathcal{O}(10\%(\epsilon^2, \delta))A_3 J_0, \end{aligned} \quad (\text{A11})$$

where the correction is some nonlinear function of J_0 , which is of order $\sim 0.1(\epsilon^2, \delta)$ times the frequency of emission, that is, for $\nu \approx 30$ GHz and $\epsilon^2, \delta \lesssim 10^{-4}$, the correction is of order a few tenths of MHz, which is smaller than the resolution element. Therefore, in this case again, we conclude that in practice, for narrow enough bandwidth, and for a resolution of a MHz or more, the comb teeth fall almost exactly at a constant spacing times $J_0 + 1/2$.

REFERENCES

- Acke B., 2011, in Joblin C., Tielens A. G. G. M., eds, EAS Publications Series Vol. 46 of EAS Publications Series, Observations of hydrocarbon emission in disks around young stars. pp 259–269
- Ali-Haïmoud Y., 2011, PhD thesis, California Institute of Technology
- Ali-Haïmoud Y., 2013, Advances in Astronomy, 2013
- Ali-Haïmoud Y., Hirata C. M., Dickinson C., 2009, Mon. Not. R. Astron. Soc., 395, 1055
- Allamandola L. J., Tielens A. G. G. M., Barker J. R., 1989, Astrophys. J. Suppl. Ser., 71, 733
- Baba M., et al., 2009, J. Chem. Phys., 131, 224318
- Bauschlicher Jr. C. W., et al., 2010, Astrophys. J. Suppl. Ser., 189, 341
- Bauschlicher Jr. C. W., Peeters E., Allamandola L. J., 2009, ApJ, 697, 311
- Boersma C., Bauschlicher C. W., Allamandola L. J., Ricca A., Peeters E., Tielens A. G. G. M., 2010, Astron. Astrophys., 511, A32
- Boersma C., Bauschlicher Jr. C. W., Ricca A., Mattioda A. L., Peeters E., Tielens A. G. G. M., Allamandola L. J., 2011, ApJ, 729, 64
- Crawford M. K., Tielens A. G. G. M., Allamandola L. J., 1985, Astrophys. J. Lett., 293, L45
- Dickinson C., et al., 2009, ApJ, 690, 1585
- Draine B. T., 2006, in Sonneborn G., Moos H. W., Andersson B.-G., eds, Astrophysics in the Far Ultraviolet: Five Years of Discovery with FUSE Vol. 348 of Astronomical

- Society of the Pacific Conference Series, Can Dust Explain Variations in the D/H Ratio?. p. 58
- Draine B. T., 2011, *Physics of the Interstellar and Inter-galactic Medium*
- Draine B. T., Hensley B., 2013, *ApJ*, 765, 159
- Draine B. T., Lazarian A., 1998a, *Astrophys. J. Lett.*, 494, L19
- Draine B. T., Lazarian A., 1998b, *ApJ*, 508, 157
- Draine B. T., Lazarian A., 1999, *ApJ*, 512, 740
- Edmonds A. R., 1960, *Angular Momentum in Quantum Mechanics*
- Hammonds M., Pathak A., Candian A., Sarre P. J., 2011, in Joblin C., Tielens A. G. G. M., eds, *EAS Publications Series Vol. 46 of EAS Publications Series, Spectroscopy of Protonated and Deprotonated PAHs*. pp 373–379
- Hudgins D. M., Bauschlicher Jr. C. W., Allamandola L. J., 2005, *ApJ*, 632, 316
- Jagod M.-F., Oka T., 1990, *Journal of Molecular Spectroscopy*, 139, 313
- Kamp I., 2011, in Joblin C., Tielens A. G. G. M., eds, *EAS Publications Series Vol. 46 of EAS Publications Series, Evolution of PAHs in Protoplanetary Disks*. pp 271–283
- Kwok S., 2004, *Nature*, 430, 985
- Kwok S., Zhang Y., 2011, *Nature*, 479, 80
- Kwok S., Zhang Y., 2013, arXiv:1304.7629
- Landau L. D., Lifshitz E. M., 1965, *Quantum mechanics*
- Le Page V., Snow T. P., Bierbaum V. M., 2003, *ApJ*, 584, 316
- Leger A., D’Hendecourt L., 1985, *Astron. Astrophys.*, 146, 81
- Li A., Draine B. T., 2012, *Astrophys. J. Lett.*, 760, L35
- Linsky J. L., Draine B. T., Moos H. W., Jenkins E. B., Wood B. E., Oliveira C., Blair W. P., Friedman S. D., Gry C., Knauth D., Kruk J. W., Lacour S., Lehner N., Redfield S., Shull J. M., Sonneborn G., Williger G. M., 2006, *ApJ*, 647, 1106
- Lovas F. J., McMahon J. R., Grabow J. U., Schnell M. and Mack J., Scott L. T., Kuczkowski R. L., 2005, *J. Am. Chem. Soc.*, pp 4345–9
- Oka T., 1995, *Journal of Molecular Structure*, 352, 225
- Peeters E., Allamandola L. J., Bauschlicher Jr. C. W., Hudgins D. M., Sandford S. A., Tielens A. G. G. M., 2004, *ApJ*, 604, 252
- Pérez L. M., et al., 2012, *Astrophys. J. Lett.*, 760, L17
- Pilleri P., Herberth D., Giesen T. F., Gerin M., Joblin C., Mulas G., Mallocci G., Grabow J.-U., Brünken S., Surin L., Steinberg B. D., Curtis K. R., Scott L. T., 2009, *Mon. Not. R. Astron. Soc.*, 397, 1053
- Pino T., Dartois E., Cao A.-T., Carpentier Y., Chamailé T., Vasquez R., Jones A. P., D’Hendecourt L., Bréchnignac P., 2008, *Astron. Astrophys.*, 490, 665
- Planck Collaboration 2011, *Astron. Astrophys.*, 536, A20
- Puget J. L., Leger A., 1989, *Annual Rev. Astron. Astrophys.*, 27, 161
- Rafikov R. R., 2006, *ApJ*, 646, 288
- Ricca A., Bauschlicher Jr. C. W., Boersma C., Tielens A. G. G. M., Allamandola L. J., 2012, *ApJ*, 754, 75
- Ritchey A. M., Federman S. R., Lambert D. L., 2011, *ApJ*, 728, 36
- Salama F., Bakes E. L. O., Allamandola L. J., Tielens A. G. G. M., 1996, *ApJ*, 458, 621
- Scaife A., 2013, *Advances in Astronomy*, 2013
- Silsbee K., Ali-Haïmoud Y., Hirata C. M., 2011, *Mon. Not. R. Astron. Soc.*, 411, 2750
- Thaddeus P., 2006, *Phil. Trans. R. Soc. B*, p. 16811687
- Thorwirth S., Theulé P., Gottlieb C. A., McCarthy M. C., Thaddeus P., 2007, *ApJ*, 662, 1309
- Tibbs C. T., Flagey N., Paladini R., Compiègne M., Shenoy S., Carey S., Noriega-Crespo A., Dickinson C., Ali-Haïmoud Y., Casassus S., Cleary K., Davies R. D., Davis R. J., Hirata C. M., Watson R. A., 2011, *Mon. Not. R. Astron. Soc.*, 418, 1889
- Tibbs C. T., Paladini R., Compiègne M., Dickinson C., Alves M. I. R., Flagey N., Shenoy S., Noriega-Crespo A., Carey S., Casassus S., Davies R. D., Davis R. J., Molinari S., Elia D., Pestalozzi M., Schisano E., 2012, *ApJ*, 754, 94
- Tielens A. G. G. M., 2008, *Annual Rev. Astron. Astrophys.*, 46, 289
- Townes C. H., Schawlow A. L., 1975, *Microwave spectroscopy*.
- van der Zwet G. P., Allamandola L. J., 1985, *Astron. Astrophys.*, 146, 76
- van Winter C., 1954, *Physica*, 20, 274
- Witt A. N., Gordon K. D., Vijh U. P., Sell P. H., Smith T. L., Xie R.-H., 2006, *ApJ*, 636, 303
- Zhang J., Han F., Pei L., Kong W., Li A., 2010, *ApJ*, 715, 485